Sensors and Actuators A 173 (2012) 293–301

Contents lists available at SciVerse ScienceDirect

Sensors and Actuators A: Physical

journal homepage: www.elsevier.com/locate/sna

Development of CNT-ISFET based pH sensing system using atomic force microscopy

Zhuxin Dong[a,*], Uchechukwu C. Wejinya[a], Siva Naga Sandeep Chalamalasetty[b]

[a] Department of Mechanical Engineering, University of Arkansas, Fayetteville, AR 72701, USA
[b] Department of Microelectronics and Photonic, University of Arkansas, Fayetteville, AR 72701, USA

ARTICLE INFO

Article history:
Received 27 May 2011
Received in revised form 25 October 2011
Accepted 30 October 2011
Available online 12 November 2011

Keywords:
CNT
DEP
AFM
ISFET
pH

ABSTRACT

In recent years, there has been an increasing interest in the monitoring and controlling of pH. It has become an important aspect of many industrial wastewater treatment processes as well as a drinking water quality issue. At the same time, the demand for smaller electronic devices used for various industrial and commercial applications has greatly increased. Nanomaterials such as Carbon Nanotubes (CNTs) are well known for their excellent electrical, mechanical, and thermal properties. Therefore, CNTs are good candidates for the manufacturing of small devices. In this paper, a novel concept combining CNT and Ion Sensitive Field Effect Transistor (ISFET) is proposed for pH-sensing application. Atomic Force Microscope (AFM) based manipulation and electrical property measurements in nano level are involved. Nanochannels are created by AFM-based nanoscratching, and the electrical properties of both multi-walled and single-walled CNTs are tested using Current Sensing AFM. FETs are fabricated to test the possibility of the CNTs' alignment between the source and the drain electrode using Dielectrophoresis (DEP). The experimental results reveal that CNT is a promising material for improving the performance and lowering the cost of existing pH chemical sensors.

1. Introduction

Carbon Nanotubes (CNTs) closely resemble hollow graphite fibers that exist in entangled bundles of tens to hundreds. They come in two different forms: Multi-Walled Carbon Nanotubes (MWCNTs) and Single-Walled carbon nanotubes (SWCNTs). SWCNTs and MWCNTs range in diameter from 1 to 10 nm and 10 to 50 nm, respectively. About 70–80% of SWCNTs tend to contain semiconducting properties, whereas 70–80% of MWCNTs tend to contain metallic properties [1–3]. CNTs have also been known to possess remarkable electrical, mechanical, and thermal properties [4]. Metallic CNTs can be used as connecting wires for Micro-Electro-Mechanical Systems (MEMS) and Nano-Electro-Mechanical Systems (NEMS) because of their size and low resistance, while semiconducting CNTs can be used for nano transistors [5].

Dielectrophoresis (DEP) is a process through which neutral particles, such as CNTs, can be translated through a suspending medium in a non-uniform electric field which is generated between a pair of electrodes. DEP is used to separate, trap, and sort cells, bacteria and other small particles. The DEP technique for aligning CNTs has been used in [3,4,6,7]. The theory and methodology have been well documented, and the method is widely used for the manipulation of particles on the micro and nano scale.

Furthermore, biomedical and chemical engineers have exploited the possibilities of chip technology to develop Si-based sensors, which have been incorporated in the tip of catheters since 1970. This technology should provide the users with cheap sensors on electronic microchips, which would become continuously cheaper, even with improved characteristics. Moreover, the reproducibility of sensor characteristics should be highly improved compared to the usually piecewise-assembled sensors due to the replication procedure on which the Si technology relies. Therefore, many of the first papers on Si sensors appeared in biomedical and chemical engineering areas. For example the previous papers addressed the development of ion sensors. The Ion Sensitive Field Effect Transistor (ISFET)-based pH sensor [8] is one of the most well-known examples, which has been already realized and applied to practice. Although so far the CNT-ISFET chemical sensor for pH monitoring has not been explored yet, we believe a proper combination may have huge potential to contribute cheaper, more compact, more efficient devices for pH sensing.

AFM was the first tool that could perform high-resolution imaging and a vacuum free working environment [9,10]. Nowadays, AFM has been playing a more important role in various research areas. This is not only because it can provide high-resolution images in both air and liquid but it is also an effective tool for the measurement of the properties, such as the mechanical properties and

* Corresponding author. Tel.: +1 497 575 4800; fax: +1 497 575 6982.
E-mail address: dzhuxin@uark.edu (Z. Dong).

0924-4247/$ – see front matter © 2011 Elsevier B.V. All rights reserved.
doi:10.1016/j.sna.2011.10.029

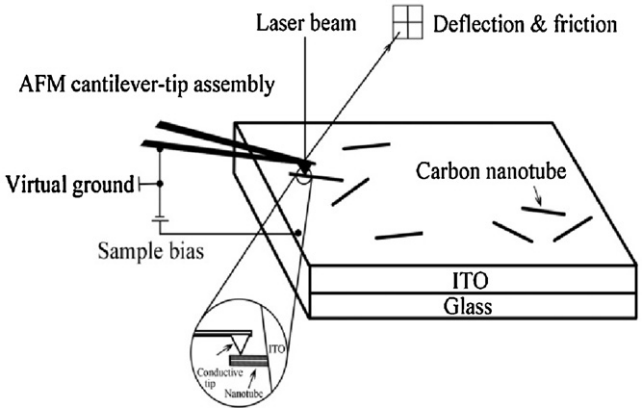

Fig. 1. Schematic of electrical properties measurement of CNTs by CSAFM.

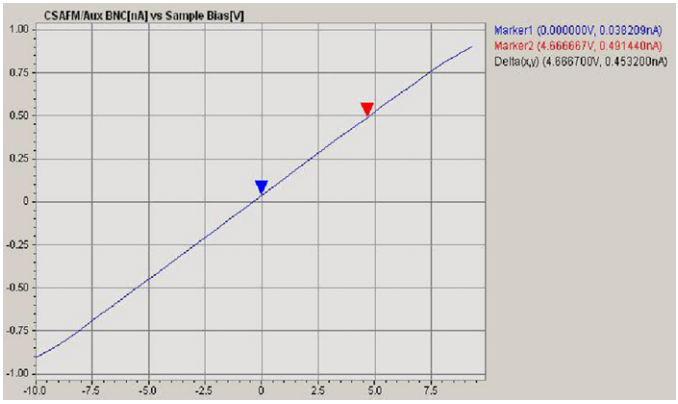

Fig. 2. Preamp plot for electrical circuit calibration.

the electrical properties, of the biomedical samples on micro/nano scale [11–13]. Thus, the electrical properties of CNTs can be determined by Current Sensing AFM (CSAFM). Additionally, the AFM tips have been employed as end effectors of robots to realize the manipulation of nanoparticles or the modification of sample surfaces [14,15]. Agilent 5500 ILM possesses a separate software package named PicoLITH which provides users with the tools necessary to perform nanolithography using an AFM tip. This enables users to either manipulate nanoparticles or scratch sample surfaces with a controllable parameter setting. Enlightened by such an advanced tool, this research is aimed at scratching the SiO_2 surface of the basic FET structure where the distance between a pair of gold microelectrodes varies. Assuming this FET was the ISFET, the gap area is also the location where the inversion layer (conducting channel) is, and this inversion layer is generated and used to transport the ions while the ISFET system is active. For instance, if there is a nanochannel inside of which the nanotubes are aligned, connecting the electrodes, the drain current between the source and the drain should be much higher under the same gate voltage. Owing to their unique electrical properties, these channel-aligned nanotubes will work as a highway for the ions and have the potential to improve the system performance dramatically. Besides, a calibration result of the AFM-based nanoscratching with two different AFM probes on Si, SiO_2, and glass surfaces is given as a reference.

In sum, we propose the idea, introduce the schematic, set up the testing, and provide the preliminary results in this paper.

2. Electrical characterization of CNT using AFM

2.1. Theory

To measure the electric properties of CNTs, we need a conductive surface to sustain the tubes. In our experiment, a glass slide is coated by an indium tin oxide (ITO) layer on the top, which guarantees the surface conductivity. A droplet of CNT solution is on the surface, and the glass wafer is dried by heating. Then the CNT sample is ready for scanning. Agilent 5500-ILM supplies a Current Sensing AFM (CSAFM) capability, where an ultra-sharp AFM cantilever, coated with conductive film, probes the conductivity and topography of the sample surface simultaneously. CSAFM requires a special 10° nose cone containing a preamplifier. A bias voltage is applied to the sample while the cantilever is kept as virtual ground. During scanning, the tip force is held constant and the current is used to construct the conductivity image of the surface. It has proven useful in joint *I–V* spectroscopy and contact force experiments as well as contact potential studies. Fig. 1 illustrates the schematic. This novel technique offers a simple and effective method with which electrical properties of single nano particle, like nanotubes, are able to be investigated.

2.2. Conductive AFM probes

The resonant frequency and spring constant of the Si AFM probes [16] are 13 kHz and 0.2 N/m respectively. These probes are coated by Cr/Pt conductively on both sides. The special nose cone assembled has a sensitivity of 10 nA/V.

2.3. Preamp

Before measuring the *I–V* curve, the electrical environment in the microscope should be examined by preamp process. A test resistor is employed to construct a connection by placing one end directly on the CSAFM nose cone, held by a spring clip, and the other to the 3-wire-EC cable that normally connects to the sample plate. Thus the test assembly takes the places of the sample and the cantilever, and then we can run a current versus bias sweep to see if the preamp is operational. The plot should of course present a linear relationship running from −1 nA to +1 nA as the voltage sweeps from −10 V and +10 V. As shown in Fig. 2, we can say the electrical circuit is reliable to carry on electrical property measurement. The plot is linear enough to validate the preamplifier. However, there is tiny offset as current in pA level is measured at 0 V. This phenomenon may be caused by imprecise parameter setting for the preamplifier and can be eliminated by further calibration. The offset is negligible as the experiment is to determine CNT is either metallic or semiconducting rather than extract exact resistance.

2.4. Testing of SWCNT

Fig. 3 shows the topography image of the surface in a 10 μm^2 area, where it is clear to find one single-walled nanotube in the middle separating from the others. After the scanning is stopped, the tip is moved to contact with the nanotube at one point of its body (see Fig. 3), and the setpoint, which controls the force of the probe acting on its target, is increased to confirm the electric connection. Next, the sample bias is modified and input in terms of range from −3 V to 3 V to draw the *I–V* curve. In Fig. 4, we can see the SWCNT has a non-linear curve of CSAFM/Aux BNC vs. Sample Bias. In CSAFM, the system has a current output range from −10 nA to 10 nA. The platform indicates the current is out of range when the bias belongs to the intervals of (−3, −1) and (1, 3). Eventually, a conclusion that the nanotube is semiconducting is established.

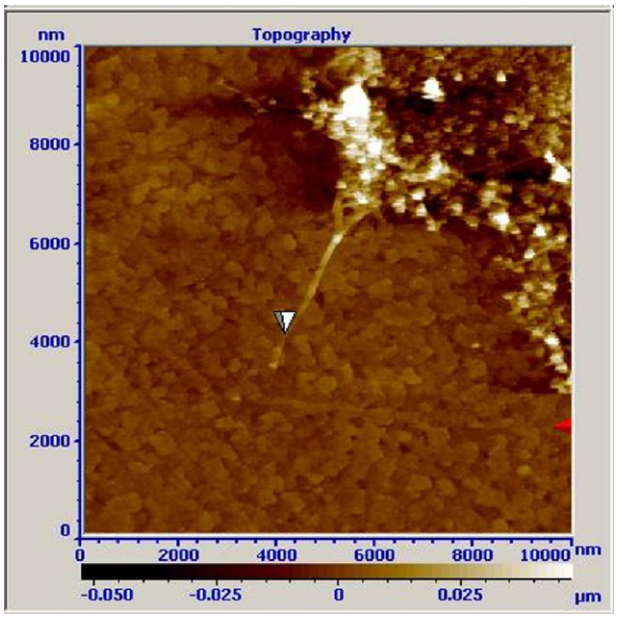

Fig. 3. Topography scan of ITO surface with SWCNTs sitting on: the position of white cursor is where the probe tip is located to measure.

2.5. Testing of MWCNT

The MWCNTs are 0.5–2 μm long and 30–50 nm in diameter. Fig. 5 illustrates the topography of the sample surface in about 1 μm^2, in the middle of which a multi-walled nanotube is forming an "island". While scanning the surface, conductivity map of the same area is also generated with a bias of 200 mV as shown in Fig. 6. This potential bias is applied from the microscope sample plate, which is connected to the ITO surface through a Cu wire. In conductivity map, larger current flows into the AFM tip in brighter area, which suggests ITO has a lower resistance than the MWCNT does. After the scanning is stopped, the tip is moved to contact with the nanotube body. The setpoint, which controls the force of the probe acting on its target, is increased to confirm the electric connection. Then the cross-section information is measured at the location as shown in Fig. 7. Fig. 8 gives the nanotube's diameter is 45 nm, which further convinces us it is a MWCNT. Finally, a potential range from −10 V to 10 V is applied to draw the *I–V* curve. In Fig. 9, we can see this MWCNT has an approximately linear relationship of CSAFM/Aux

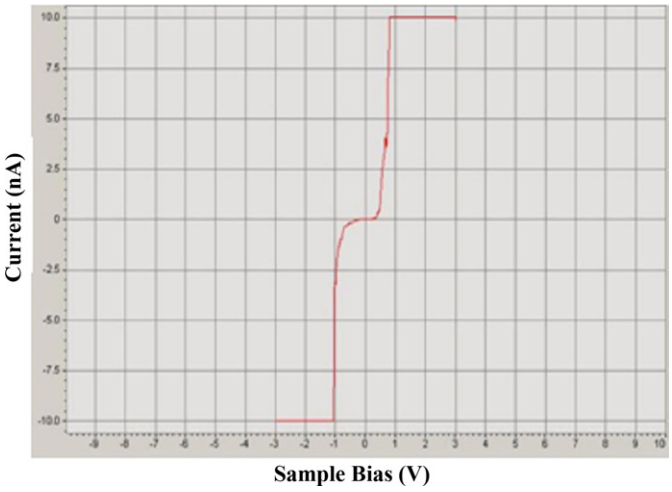

Fig. 4. *I–V* curve measurement on SWCNT body with bias from −3 to +3 V.

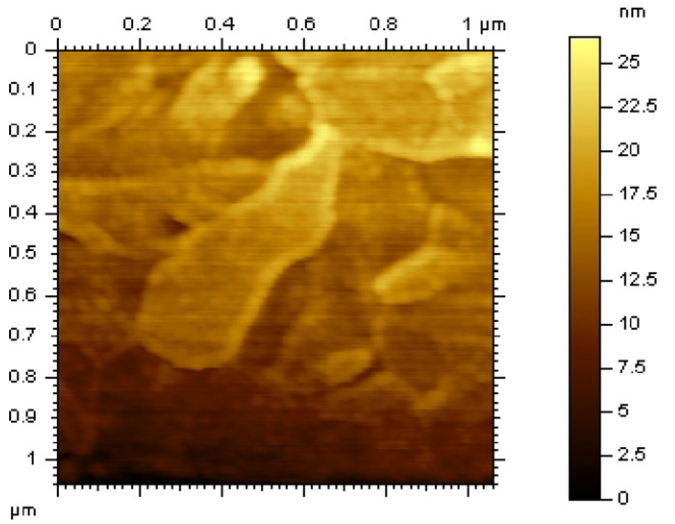

Fig. 5. Topography scan of ITO surface with MWCNTs sitting on.

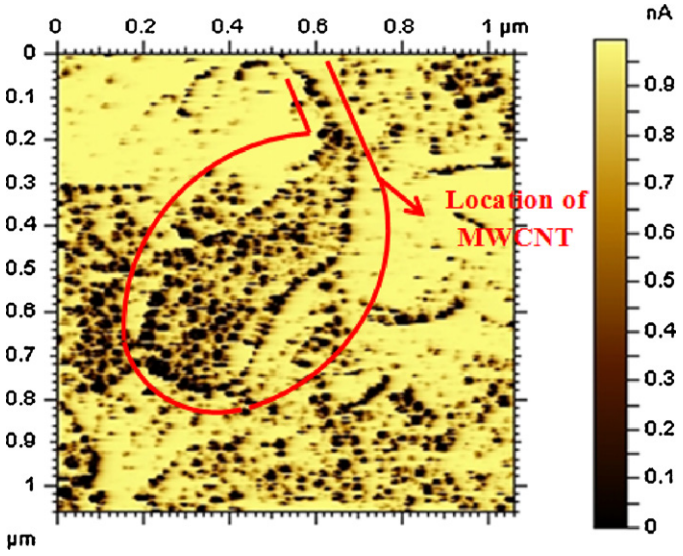

Fig. 6. Conductivity map obtained at bias of 200 mV.

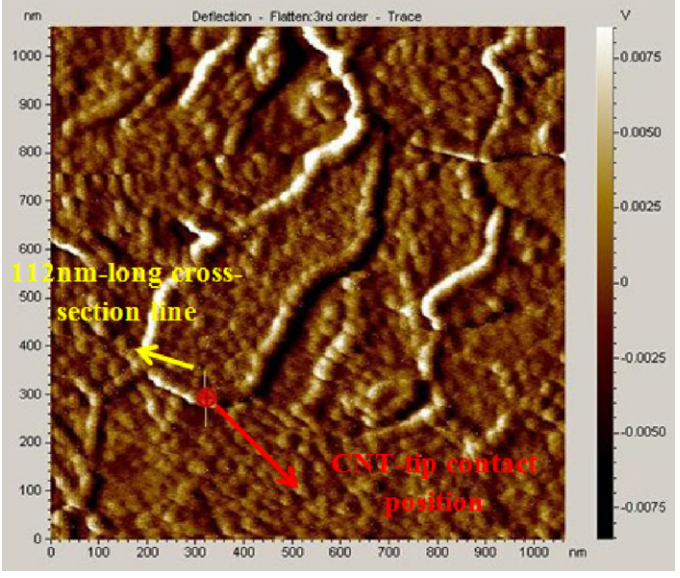

Fig. 7. Deflection scam image shows the contact position on the CNT body.

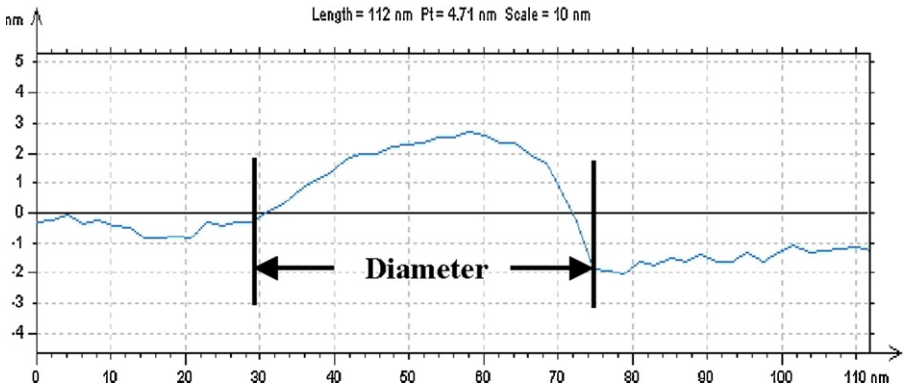

Fig. 8. A 112 nm-long cross-section line for CNT size measurement.

BNC vs. Sample Bias. Eventually, a conclusion that the MWCNT is metallic is established.

3. CNT-based ISFET

3.1. ISFET

An ISFET is generally used to measure ion concentrations in solutions. When the ion concentration, such as pH, changes, the current through the transistor will change accordingly. Researchers have reported ISFET development for sensing ion concentration in solutions for more than 30 years [17–19]. Solution is used as the gate electrode instead of the traditional metal gate. The voltage between substrate and oxide surfaces arises due to an ions' sheath. An ISFET's source and drain are constructed similar to a Metal-oxide Semiconductor Field-Effect Transistor (MOSFET) [20]. Although an ISFET is similar to a MOSFET, there are still some differences. As shown in Fig. 10, the metal gate is replaced by the metal of a reference electrode, while the target liquid in which this electrode is present makes contact with the bare gate insulator. Both have the same equivalent circuit. Devices with this structure can be applied to pH measurement. However, the final objective of our work on the nano-pH sensor is to enhance the inversion layer with CNTs as "nano-bridge" to conduct electrons between the drain and source. The drain current might be much greater under the same condition. When ISFET device is active, ions will flow between the source and drain through the inversion layer and form the drain current, whose magnitude depends on the ion concentration of solution. CNT-ISFET structure intends to make use of CNTs' extremely high current carrying capacity (~1 TA/cm^3) to improve the performance. There will be a "highway" for the ions after CNTs are aligned properly inside a nanochannel that is fabricated in the location of the inversion layer. Fig. 11 illustrates the design for CNT-ISFET structure

Fig. 9. *I–V* curve measurement on MWCNT body with bias from −10 to +10 V.

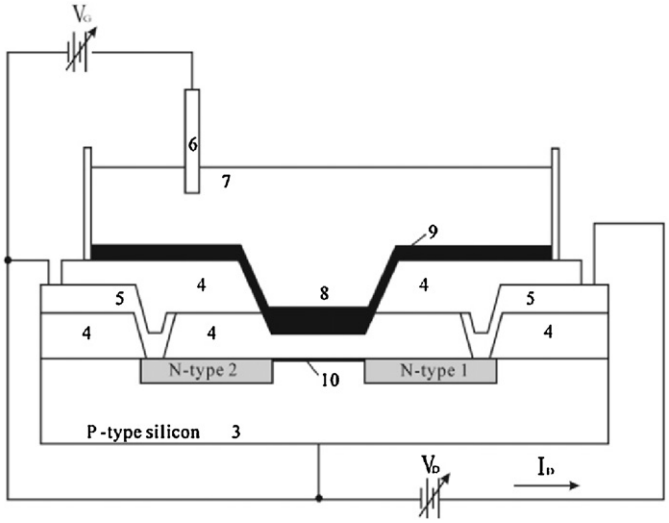

Fig. 10. Schematic ISFET: 1 drain; 2 source; 3 Si; 4 SiO_2; 5 metal; 6 reference electrode; 7 solution; 8 electroactive membrane; 10 inversion layer membrane.

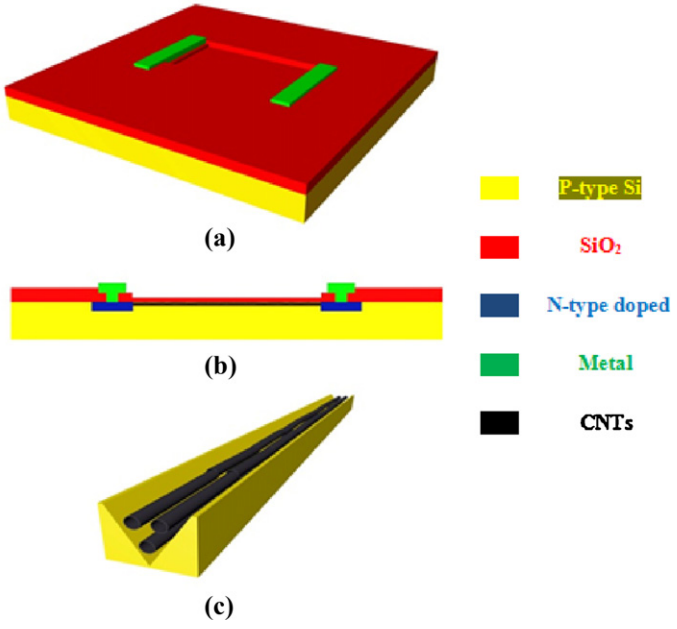

Fig. 11. Structure design of CNT-ISFET pH sensing device: (a) perspective view, (b) side view and (c) CNTs in nanochannel.

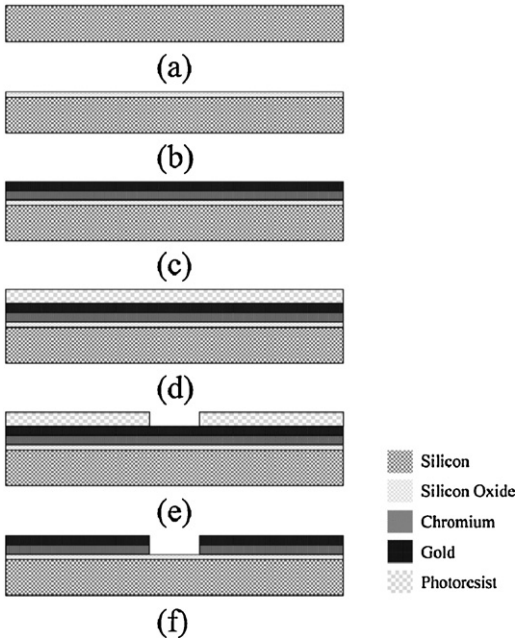

Fig. 12. Fabrication process of micro electrode: (a) Si substrate; (b) 300 Å SiO_2 by thermal oxidation of Si wafer; (c) both chromium and gold are deposited on the SiO_2 surface by evaporation and electro plating; (d) cover the surface by photoresist layer; (e) photoresist is patterned and exposed; (f) the metals are etched as patterned and the rest of photoresist is stripped off completely.

with nanochannel. If all of these conditions are satisfied, then these devices could be fabricated and manufactured cost-efficiently.

3.2. FET fabrication

The basic FET structure is originally made up of four layers from bottom up: Si wafer, 300 Å of SiO_2, 200 Å of chromium and 5000 Å of gold, using MEMS surface micromachining techniques. The fabrication flowchart is illustrated in Fig. 12. For the electrode fabrication, a mask as shown in Fig. 13 is first designed for the desired chips. Triangular electrodes of 30, 60 and 90° angles, with electrode gaps

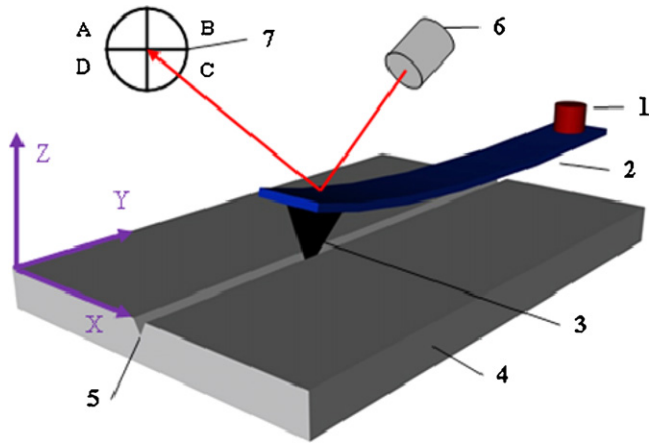

Fig. 14. Schematic of AFM-based nanoscratching: 1 piezo scanner for XYZ movement, 2 cantilever, 3 tip, 4 SiO_2, 5 nanochannel, 6 laser and 7 four-quadrant PSD.

of different lengths are designed. 24 microelectrode chips are fitted on a circular Si wafer with a diameter of 125 mm. The reason why we chose triangular variation is that triangular variation provides a wider zone of stronger DEP force and weaker hydrodynamic force than other variations, such as square and semicircular-shaped ones, which do not allow particles to be easily released [21].

4. AFM-based surface nanoscratching

Since the basic FET structure has been fabricated on the chip, the AFM-based surface nanoscratching process can readily be carried out. A chip with nine pairs of gold microelectrode is scratched by a Diamond-Like-Carbon (DLC) coating AFM tip [22] at the location of the electrode gaps. Each pair of electrode has a 60° triangle shape with about 20 μm gap, and the DLC tip is of a 48 N/m spring constant and a 190 kHz resonant frequency. Fig. 14 illustrates the schematic of AFM-based surface nanoscratching. Before scratching SiO_2 surface, a topography scan of the area, which encloses the location of desired nanochannel is necessary. Fig. 15 shows an AFM topography scan of a pair of electrodes under contact imaging mode. This image is then loaded into PicoLITH and ready for

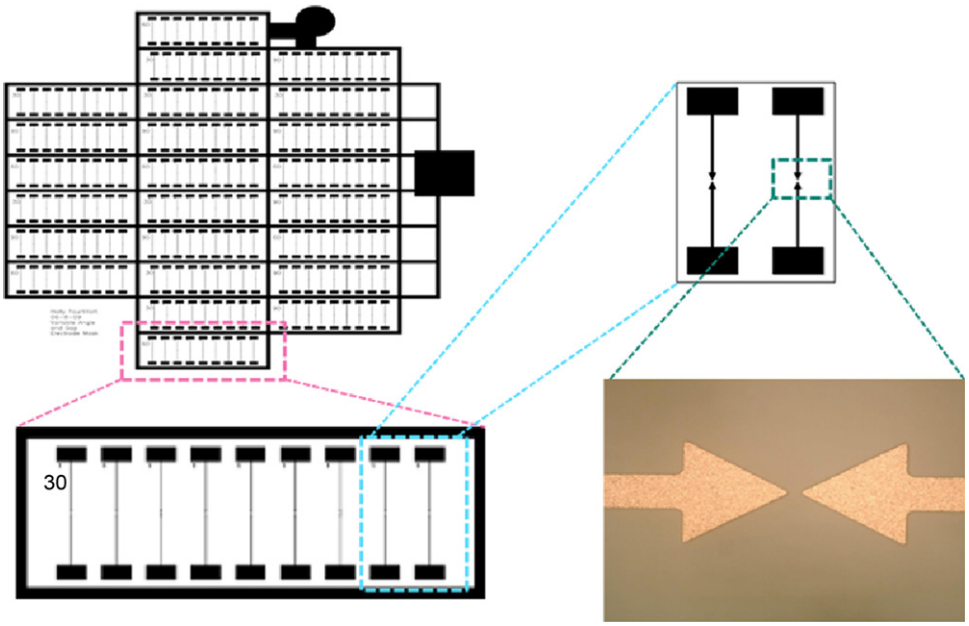

Fig. 13. Mask design and Au microelectrodes on Si substrate as FET.

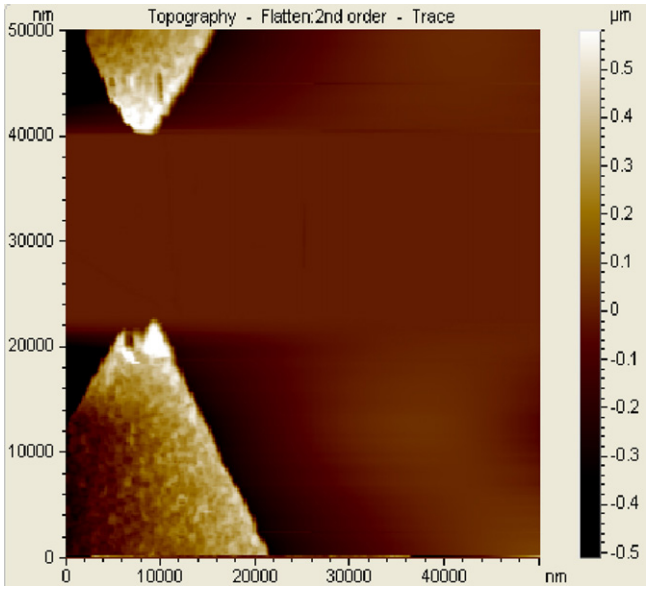

Fig. 15. AFM topography image of a pair of electrodes before scratching.

scratching. The object can be drawn on the loaded image and the parameters for the nanochannel are set as follows: force setpoint at 7.5 V, which will maintain a constant mechanical force between the AFM tip and the surface by maintaining a constant amount of deflection of the cantilever for the entire manipulation and has a range of −10.0 V to 10.0 V; tip speed is 2 μm/s during the manipulation, and it varies depending on the length of the nanochannel; and 75 times for scratching. In this experiment, the object is drawn as a straight line between the two electrodes. By positioning the tip to the start point where the object starts, the nanochannel gets started. Fig. 16 presents the 3-dimensional topography scan after scratching the electrode gap. As we can see, there is a clear channel scratched between the two electrodes and the width and depth of the channel can be measured as shown in Fig. 17. On this chip, eight out of nine pairs of electrode gaps were cut except for the one in the middle (5th pair). Table 1 provides the details of the dimension measurement of the nano channels. These channels are embedded so they can be regarded as an enhanced inversion layers after filled with CNTs properly, and we expect an improvement of the structure performance.

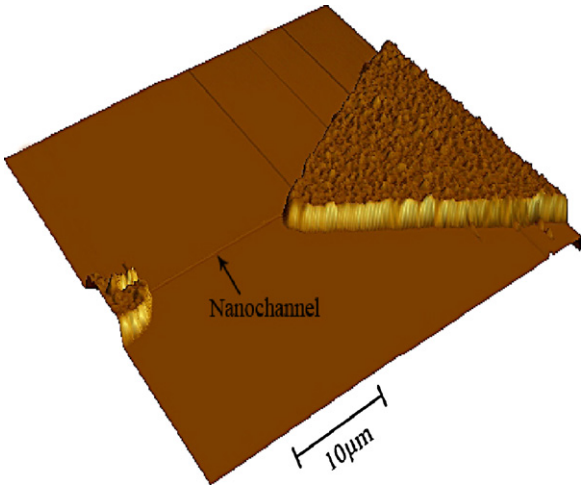

Fig. 16. 3D topography image of a pair of electrodes with scratched gap.

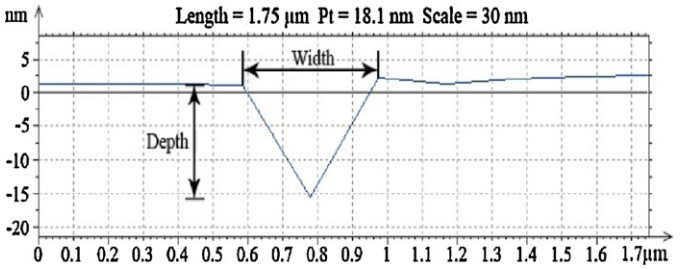

Fig. 17. Dimension measurement of a scratched nanochannel.

5. Characterization of CNT-FET electrical property

5.1. CNT preparation

Two CNT-samples are prepared: 1.37 mg SWCNTs dissolved in 1 ml Deionized (DI) water with 2 μl Triton; and 2.69 mg MWCNTs dissolved in 1 ml DI water with 5 μl Nanosperse. Then both samples are sonicated for 1 h. After the stocks are available, 5×, 10× and 20× dilutions are also prepared.

5.2. Wire bonding

For wire bonding, since the traditional method of soldering can damage microchips easily, conductive epoxy is used to stick wires onto the gold (Au) pads in order to interface the outer environment. In the experiment, the two parts of conductive epoxy are equally mixed, and then we deposit a little of the mixture on the pads. Finally, the wires can be stuck to the pads. The epoxy will get firm enough to bond stably after being heated at 130 °C for about 1 h on a heat plate. Eventually, we have wires ready coming from the Au pads to apply DEP forces in between the electrodes.

5.3. CNT alignment

Fig. 18 illustrates the experimental setup for CNT alignment by applying DEP forces. A function generator provides us with an AC power of 20 $V_{p\text{-}p}$ and 1.5 MHz, which will be verified by the oscilloscope. Then the chip is real-time observed by the optical microscope during the alignment. 1.5 μl of 10× SWCNT dilution is dropped on the gap of the electrode pairs 1–4 while 1.5 μl of 10× MWCNT dilution for the pairs 6–9. Then by connecting the electrodes to the function generator, DEP forces are generated in the gaps, and the electrodes are bridged by the CNTs. Fig. 19 shows the observations of the electrode gaps.

5.4. Electrical property measurement

For testing *I–V* characteristics, the gap distance is about 20 μm, and a pipette, whose sucking range is from 0.5 to 10 μl, is used

Table 1
Dimension measurement results of scratched nanochannels.

Elec. Pair #	Length (μm)	Width (μm)	Depth (nm)
1	17.32	0.58	2.8
2	21.88	0.39	2.10
3	18.16	0.59	4.90
4	18.75	0.59	9.10
6	21.09	0.78	3.40
7	17.97	0.39	4.21
8[a]	18.95	0.39	16.80
9	19.14	0.39	1.80
Average	19.16	0.513	5.64

[a] As shown in Fig. 16.

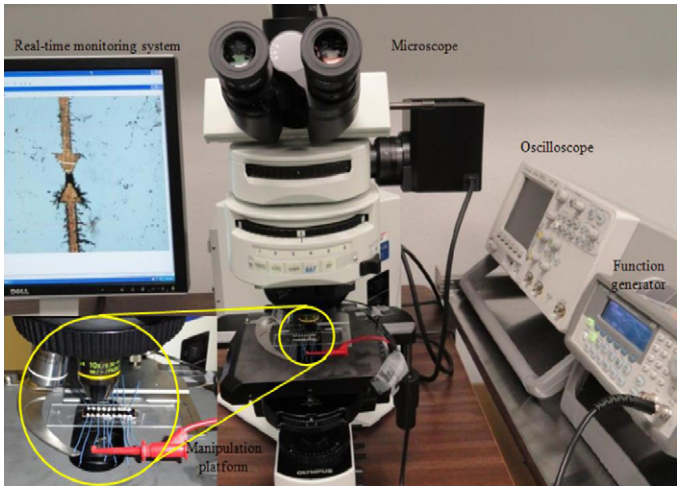

Fig. 18. Experimental setup for DEP application.

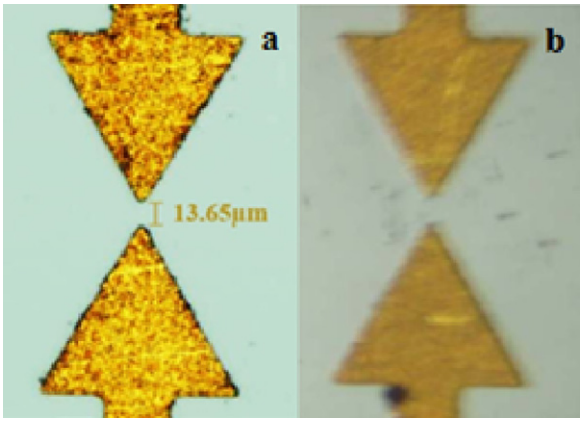

Fig. 19. Pairs of Au electrodes observed by optical microscope: a. gap measure; b. covered by tiny CNT droplet.

to deposit a 1.5 μl CNT droplet from the 10× dilutions onto the gaps. Fig. 20 shows *I–V* curve measurement results of all the nine pairs of electrodes. As we can see, both SWNTs and MWNTs aligned between the gaps possess a linear *I–V* curve. This linear relationship

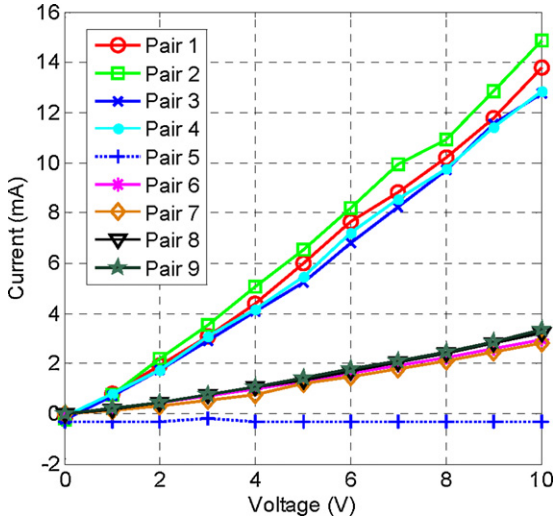

Fig. 20. *I–V* curve measurement with SWCNTs alignment (Pair 1–4) and MWCNTs alignment (Pair 6–9) in the scratched gaps. Pair 5 is for the bare electrode.

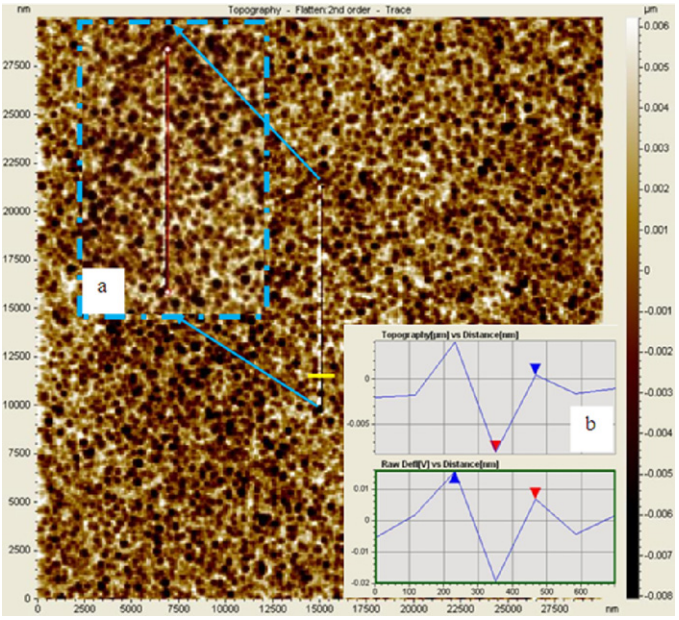

Fig. 21. Re-image the topography of workspace: a nanochannel on Si substrate; a. the real channel locally overlaps the desired one in red; b. channel dimension. (For interpretation of the references to color in this figure legend, the reader is referred to the web version of the article.)

reveals that these CNTs are metallic and possessing very excellent ion conductive properties. Once ISFET is activated and the ions are generated between the source and drain, this CNT-based enhanced inversion layer will allow a lot more ions to go through it. Therefore, the drain current should increase accordingly.

6. Calibration of nanoscratching with two kinds of AFM probes

The calibration is used to specify the effect of two kinds of AFM probes when they are used to create nanochannels on Si, SiO_2 and glass surfaces. The AFM probes are Tap190DLC [22] and PPP-NCH [23], both of which are recommended by the manufacturers for nanoscratching. In the experiment, the scratching is completed under the close-loop mode in order to guarantee precise control of location. The results can help us to judge preliminarily whether these probes are capable of creating nanochannels in the CNT-ISFET system.

6.1. Calibration of Tap190DLC

As introduced in the previous chapter, this tip has a 48 N/m force constant and a 190 kHz resonant frequency. In general, a 48 N/m probe is almost the stiffest one available in the current market. Two channels are made in different settings on Si, SiO_2, and glass respectively. Five measurements are taken on each channel for the width and depth. Table 2 provides the parameters and measurements of the nanochannels, which tells Tap190DLC is able to create nanochannels on all the three materials (M.). However, it is inefficient, especially when scratching on the Si surface. For example, 150 times for an 11.7188 μm channel at 1.5 μm/s speed (Sp.) takes about 45 min and only provides a 5 μm-deep channel. Table 2 also proves that the setpoint (Spt.) and time (T) are the two key factors that determine the depth of the channel. Fig. 21 presents a precise control of the channel location: the real channel is right underneath the red line that shows the desired channel after scratching under the close-loop mode.

Table 2
Calibration results of Tap190dlc on Si, SiO_2 and glass.

M.	Spt.(V)	Sp. (μm/s)	Time	Ave. W. (nm)	Stdev. W	Ave. D. (nm)	Stdev. D.
Si	7.5	1.5	150	233	0.632	4.94	2.88
Si	7.5	1.5	100	NA	NA	NA	NA
SiO_2	7.5	1.5	100	350	0	39.5	6.85
SiO_2	7.5	1.5	50	362	150	0.446	0.101
SiO_2	5	1.5	100	NA	NA	NA	NA
G	7.5	1.5	100	362	66.4	7.76	2.29
G	7.5	1.5	50	280	60.5	0.912	0.354
G	5	1.5	100	NA	NA	NA	NA

NA represents no channel.

Table 3
Calibration results of PPP-NCH on Si, SiO_2 and glass.

M.	Spt.(V)	Sp. (um/s)	Time	Ave. W. (nm)	Stdev. W	Ave. D. (nm)	Stdev. D.
Si	8	2	150	NA	NA	NA	NA
SiO_2	7.5	1.5	100	NA	NA	NA	NA
G	7.5	1.5	100	1576	420	-40.5	16.9

- indicates the height instead of the depth.

6.2. Calibration of PPP-NCH

PPP-NCH has a lower force constant of 42 N/m, and as shown in Table 3, we are unable to create nanochannels on any of the three samples even though the setpoint is increased to 8 V. Additionally, the glass surface heaves in the track that the tip scratches as shown in Fig. 22. During all the attempts with PPP-NCH, there is no channel, but the heaving phenomenon also appears on Si substrate. Besides the force constant and the resonant frequency, another important difference between the two tips is that Tap190DLC has a 15 nm-thick diamond-like-carbon coating to protect the tip while PPP-NCH does not, which means scratching with PPP-NCH will leave some residuals of the tip on the surface, and scratching with Tap190DLC leaves nothing. Therefore, in comparison to PPP-NCH, Tap190DLC is more suitable for this specified task. In the future, a tip with diamond coating [24–26] is necessary for deep channels with acceptable stability and efficiency.

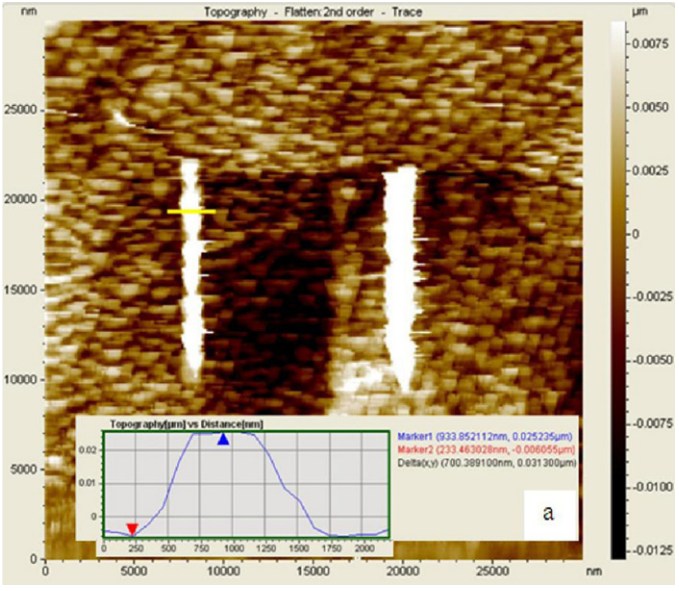

Fig. 22. Re-image the topography of workspace: two nanochannels are created on glass but, unexpectedly, both are above the surface; a. channel dimension.

7. Conclusion

In this paper, we proposed a novel idea about a combination of CNTs and ISFET structure for the improvement of pH-sensing. FET structure was fabricated and CNTs were aligned by DEP in order to prove the feasibility of the connection between the source and the drain. The CSAFM concept and schematic were introduced to show the electrical properties of CNTs, and with this method the electrical properties of both MWCNT and SWCNT were determined. Furthermore, the calibration of two kinds of AFM tips scratching on three different surfaces was completed, and the calibration results revealed that Tap190DLC was the suitable one for creating nanochannels on Si, SiO_2, and glass substrates. However, in order to obtain deep channels on Si efficiently, a specified tip for nanoindenting/nanoscratching applications with a diamond tip apex was recommended.

Ongoing research has been focusing on the fabrication of ISFET chip, and CNTs will be embedded into the system using AFM-based nanoscratching during the fabrication procedures.

References

[1] E. Katz, I. Willner, Biomolecule-functionalized carbon nanotubes: applications in nanobioelectronics, Chem. Phys. Chem. 5 (2004) 1084–1104.
[2] A. Javey, J. Guo, Q. Wang, M. Lundstrom, H. Dai, Ballistic carbon nanotube field-effect transistors, Lett. Nat. 424 (August) (2003) 654–657.
[3] J. Clendenin, J. Kim, S. Tung, An aligned carbon nanotube biosensor for DNA detection, in: Proceedings of the 2nd IEEE International Conference on Nano/Micro Engineering and Molecular Systems (NEMS), Bangkok, Thailand, January 16–19, 2007.
[4] L. Dong, A. Subramanian, B. Nelson, Carbon nanotube for nano robotics, Nano Today 2 (December (6)) (2007).
[5] K. Lai, N. Xi, U. Wejinya, Y. Shen, W.J. Li, Automated robotic deposition for manufacturing nano devices, in: Proceedings of the 2007 IEEE/RSJ International Conference on Intelligent Robots and Systems, San Diego, CA, USA, 29 October–2 November, 2007.
[6] A. Ramos, H. Morgan, N. Green, A. Castellanos, Ac electrokinetics: a review of forces in microelectrode structures, J. Phys. D: Appl. Phys. 31 (September) (1998) 2338–2353.
[7] U. Wejinya, N. Xi, Y. Shen, K. Lai, Modeling dielectrophoretic force for manipulating carbon nanotubes, in: Proceedings of the 2007 IEEE/ASME International Conference on Advanced Intelligent Mechatronics, Zürich, Switzerland, September, 2007.
[8] P. Bergveld Em, ISFET theory and practice, in: Proceeding of IEEE Sensor Conference, Toronto, Canada, October 22–24, 2003.
[9] G. Binning, C.F. Quate, C. Gerber, Atomic force microscope, Phys. Rev. Lett. 56–9 (1986) 930–933.
[10] D.M. Schaefer, R. Reifenberger, A. Patil, R.P. Andres, Fabrication of two-dimensional arrays of nanometer-size clusters with the atomic force microscope, Appl. Phys. Lett. 66 (1995) 1012–1014.

[11] Z. Dong, U.C. Wejinya, Y. Zhuxin, K. Ye, Force measurement study of engineered collagen-chitosan scaffold using atomic force microscopy, in: Proceedings of 2010 IEEE International Conference on Nano/Molecular Medicine and Engineering (NANOMED), Hong Kong/Macau, China, December 5–9, 2010.
[12] BoBae Lee, Lin Han, H. Eliot, Frank., Dynamic mechanical properties of the tissue-engineered matrix associated with individual chondrocytes, J. Biomech. 43 (2010) 469–476.
[13] M.B. Schulte, Z. Dong, S. Tung, J.-W. Kim, U.C. Wejinya, H.-M. Moon, B.-W. Kong, Impedance spectroscopy of chicken infectious laryngotracheitis virus based on atomic force microscopy, in: Proceedings of the 2009 IEEE 3rd International Conference on Nano/Molecular Medicine and Engineering (NANOMED), Tainan, Taiwan 21, October 18, 2009.
[14] G. Li, N. Xi, M. Yu, W. Feng, Development of augmented reality system for AFM-based nanomanipulation, in: Mechatronics, IEEE/ASME Transactions on Mechatronics, vol. 9, 2004, pp. 358–365.
[15] G. Li, N. Xi, D.H. Wang, In situ sensing and manipulation of molecules in biological samples using a nano robotic system, Nanomedicine 1 (1) (2005) 31–40.
[16] URL:http://www.budgetsensors.com/downloads/ElectriCont_Datasheet.pdf.
[17] S.C. Chen, Y.-K. Su, J.S. Tzeng, The fabrication and characterization of ion-sensitive field effect transistors with a silicon dioxide gate, J. Phys. D: Appl. Phys. 19 (1986) 1951–1956.
[18] P. Bergveld, Thirty years of ISFETOLOGY What happened in the past 30 years and what may happen in the next 30 years, Sens. Actuators B 88 (2003) 1–20.
[19] P. Bergveld, ISFET theory and practice, in: Proceedings of IEEE Sensor Conference, Toronto, October, 2003, p. 26.
[20] H.C. Casey Jr., Devices For Integrated Circuits-Si and III-V Compound Semiconductors, 8, John Wiley & Sons, Inc., 1999, pp. 342–426.
[21] L. Yu, C. Iliescu, G. Xu, F.E.H. Tay, Sequential field-flow cell separation method in a dielectrophoresis chip with 3-D electrodes, J. Microelectromech. Syst. 16 (October (5)) (2007).
[22] URL:http://www.budgetsensors.com/downloads/Datasheet_Tap190DLC_EN.pdf.
[23] URL:http://www.home.agilent.com/upload/cmc_upload/All/PointProbe_Plus.pdf?&cc=US&lc=eng.
[24] URL:http://www.brukerafmprobes.com/p-3385-pdnisp.aspx.
[25] Z. Wang, S. Tung, N. Jiao, Z. Dong, Nanochannels on silicon oxide surface fabricated by atomic force microscopy, in: Proceedings of the 5th IEEE International Conference on Nano/Micro Engineered and Molecular Systems (NEMS), Xiamen, China, January 20–23, 2010.
[26] Z. Wang, S. Tung, N. Jiao, Z. Dong, A nanochannel system fabricated by MEMS microfabrication and atomic force microscopy, in: Proceedings of the 6th IEEE International Conference on Nano/Micro Engineered and Molecular Systems (NEMS), Kaohsiung, Taiwan, February 20–23, 2011.